



Article

Li Chemical and Tracer Diffusivities in LiCoO₂ Sintered Pellets

Erwin Hüger ^{1,2,*} and Harald Schmidt ^{1,2} ¹ Solid State Kinetics Group, Institute of Metallurgy, Clausthal University of Technology, 38678 Clausthal-Zellerfeld, Germany; harald.schmidt@tu-clausthal.de² Clausthal Center for Materials Technology, 38678 Clausthal-Zellerfeld, Germany

* Correspondence: erwin.hueger@tu-clausthal.de

Abstract: LiCoO₂ (LCO) is a crucial active material for positive electrodes of commercial lithium-ion batteries. It is typically present in the form of micrometer-sized LCO particles, which are surrounded by binders and conductive agents with a thickness of tens of microns. In order to determine the intrinsic Li transport parameters of pure crystalline LCO, it is necessary to measure the Li diffusivity at room temperature in sintered LCO pellets free of additives. The LCO sintered bulk material consists of interconnected, about 3 μm clusters, composed of grains of about 70 nanometers in size. The Li chemical and tracer diffusivities are determined using electrochemical impedance spectroscopy (EIS) and potentiostatic intermittent titration technique (PITT), while the latter ones are in the range between 10⁻⁹ and 10⁻²⁸ m²s⁻¹, depending on the application of different relevant formulas and characteristic parameters. Consequently, it is essential to apply a classical non-electrochemical and Li selective method of tracer diffusion determination like ⁶Li depth profiling and secondary ion mass spectrometry (SIMS) for comparison. Li tracer diffusivities of about 10⁻²² m²s⁻¹ at room temperature are obtained by the extrapolation of the SIMS results from higher temperatures. This significantly narrows the range of reliable electrochemically determined Li tracer diffusivities to a more limited range, between 10⁻²¹ and 10⁻²² m²s⁻¹.

Keywords: LiCoO₂; diffusion; thermodynamic factor; EIS; PITT; SIMS; LIB; cathode materials

Citation: Hüger, E.; Schmidt, H. Li Chemical and Tracer Diffusivities in LiCoO₂ Sintered Pellets. *Batteries* **2024**, *10*, 446. <https://doi.org/10.3390/batteries10120446>

Academic Editor: Yong-Joon Park

Received: 30 October 2024

Revised: 11 December 2024

Accepted: 12 December 2024

Published: 16 December 2024



Copyright: © 2024 by the authors. Licensee MDPI, Basel, Switzerland. This article is an open access article distributed under the terms and conditions of the Creative Commons Attribution (CC BY) license (<https://creativecommons.org/licenses/by/4.0/>).

1. Introduction

In order to accurately describe lithium-ion battery (LIB) performance, it is essential to understand and quantify not only the charge/discharge behaviour, but also the process of solid-state diffusion in electrodes that regulates the kinetics of this behaviour [1]. The diffusion of Li has a direct impact on the charge/discharge times (and consequently on the power density), the maximum capacity, the generation of stress (electrode stability), and the occurrence of side reactions. This was demonstrated by experiments on lithium cobalt oxide (LiCoO₂), referred to as LCO, which is a well-established cathode (positive electrode) active material in commercial LIBs [2,3].

LCO is a layered material comprising lithium oxide (001) atomic layers and cobalt oxide (001) atomic layers stacked sequentially along the crystallographic c-axis [2,3]. It is assumed that rapid Li diffusion will occur within the lithium oxide layers (i.e., in the ab-plane) where Li vacancies are present. In the direction perpendicular to the lithium oxide layers, i.e., in the c-axis direction, Li has to permeate through the cobalt oxide layers, which produces a low Li flux (low Li⁺ current) due to the lack of Li vacancies in the cobalt oxide layers. This may be considered as an almost blocked Li diffusion perpendicular to the cobalt oxide layer (in the c-axis direction) [4]. Recent Li tracer diffusion experiments on LCO single crystals based on secondary ion mass spectrometry (SIMS) have corroborated this hypothesis [5]. The fast Li diffusivity path perpendicular to the c-axis may facilitate the extraction and insertion of Li⁺ into LCO, which is of interest for the operation of LIBs. The impact of the Li diffusivity anisotropy in LCO on LIB performance has also been demonstrated by electrochemical experiments. In films of LCO oriented along the c-axis

(where the c-axis is perpendicular to the electrolyte/film interface), the capacity and rate capability were observed to be inferior to those of LCO films where the c-axis is parallel to the electrolyte/film interface [6]. The high-rate capacity is dependent on the presence of fast Li diffusion paths that are perpendicular to the electrolyte/cathode interface. This has been demonstrated in (104) (ab-plane) oriented LCO films. In the case of polycrystalline LCO, the Li diffusivity was determined in sintered polycrystalline bulk LCO pellets [5,7] and in polycrystalline LCO thin films [4,6,8]. The Li diffusivity in polycrystalline LCO was found to be faster than in c-axis oriented LCO films and single crystals, and similarly faster than in ab-plane oriented LCO single crystals [5].

A highly convenient methodology for the determination of the Li diffusivity in LIB electrodes employs electrochemical-based measurement techniques, including electrochemical impedance spectroscopy (EIS) [9–32] and pulse methods such as potentiostatic intermittent titration technique (PITT) [4,9,23,33,34] and galvanostatic intermittent titration technique (GITT) [23,35]. All these methods offer the advantage of being applied *in situ*, without the need for cell disassembly or electrode washing procedures. At least for PITT and GITT techniques, measurements can be performed during LIB operation, a process referred to as *operando* measurements. A recent review article provides an overview of how these electrochemically based methodologies are applied to determine the Li diffusivity [9]. Using SIMS [9,36–38] the diffusivities are directly determined by measuring the diffusion induced modification of a ${}^6\text{Li}$ tracer distribution during annealing [9]. In contrast, electrochemical methods are more indirect, involving the application of different models resulting often in contradictory results. In electrochemical experiments, the observed signal may not be exclusively attributable to Li diffusion within the active material. Rather, it may also be influenced by other processes, including electrolyte/surface polarization. Accordingly, the Li diffusivities derived in this study may not fully reflect the diffusion process occurring in the cathode active material. See reference [9] for a detailed discussion of this topic. The objective of the present study is to use the diffusivity data acquired by SIMS depth profiling to evaluate the results obtained from electrochemical methods.

The SIMS method has the following advantages for Li diffusivity determination. First, Li easily loses its valence electron (high ionisation cross section), which results in Li^+ SIMS signals of relatively high intensity. A further advantage is that it can discriminate between the two stable Li isotopes, which enables Li selective tracer studies. A third reason is that, in contrast to nuclear magnetic resonance (NMR) spectroscopy, which is also employed to determine diffusivities, SIMS is not influenced by the magnetic element cobalt. The fourth and fifth reasons pertain to a comparison of SIMS with the established electrochemical methodologies of GITT/PITT and EIS. These methods are typically only applicable at or near room temperature, thus providing no insight into activation energies and the underlying defect structure. Furthermore, they lack selectivity for lithium. Electrochemical measurements of diffusivities may involve interfacial processes, (parasitic) electronic currents, ohmic resistances, and side reactions that frequently interfere with the analysis. In contrast, tracer methods provide a direct measurement of the Li tracer diffusion coefficient, eliminating the need for model-dependent correction factors.

Table 1 of reference [4] presents a literature overview of the diffusivities of Li in LCO electrodes, as determined via EIS, PITT, and GITT at room temperature. These electrodes were prepared by two methods: deposition of thin films and drying slurries of an ensemble of LCO powder particles with binder and conductive additives to form a surrounding layer with a thickness in the tens of microns. The diffusivities span a range from 10^{-11} to $10^{-15}\text{ m}^2\text{s}^{-1}$, which is significantly higher than the tracer diffusivities at room temperature (Figure 1). The discrepancy can be attributed to the following factors: (i) the application of different models (e.g., different equations) to extract diffusivities and (ii) the difference between chemical and Li tracer diffusivities by the thermodynamic factor (TF), (iii) differing preparation procedures (e.g., the use of different electrode additives), and (iv) different state-of charge (SOC) of the electrode.

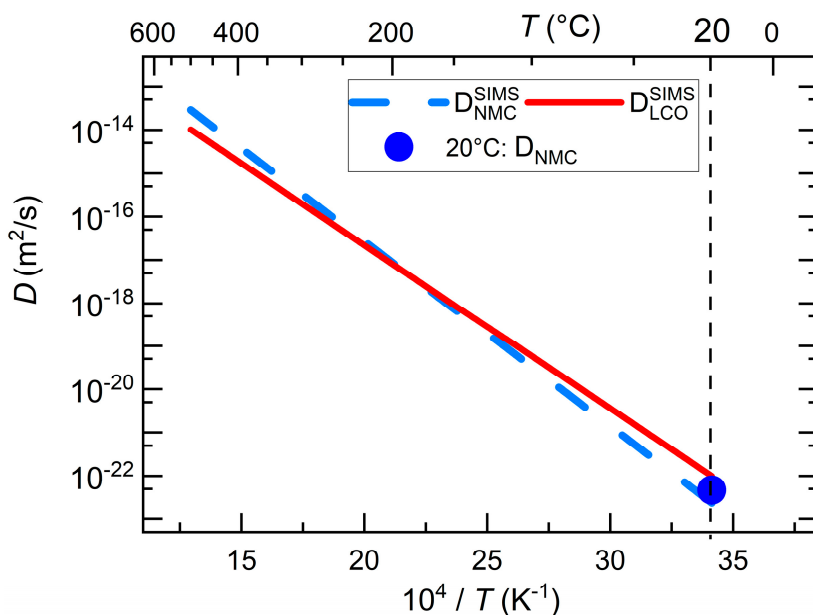


Figure 1. Arrhenius plot of the Li tracer diffusivities of LCO and NMC111 as determined from SIMS depth profiling on sintered pellets. The plots were obtained as described in the main text. The Li diffusivities were experimentally determined between 100 °C and 400 °C for NMC and between 200 °C and 500 °C for LCO. The values below 100 °C for NMC and below 200 °C for LCO are extrapolated values derived in accordance with the Arrhenius law. The blue dot at 20 °C represents the Li diffusivity in the sintered NMC111 pellet, which was determined to be $(4.7 \pm 1.9) \times 10^{-23} \text{ m}^2 \text{s}^{-1}$ by SIMS in a long-term (800 days) experiment performed at room temperature.

LCO represents one of the corners of the class of layered positive electrode materials, which includes NMC ($\text{LiNi}_x\text{Mn}_y\text{Co}_z\text{O}_2$, where $x + y + z = 1$). All of these materials are of interest as cathode materials for LIBs [2,9]. Of the corner materials, i.e., LiNiO_2 ($x = 1$) [39], LiMnO_2 ($y = 1$), and LCO ($z = 1$) [5], LCO is the most stable material during LIB operation and thus one of the well-established materials in commercial LIBs [2,3]. LCO is a suitable cathode material due to the high electrochemical potential of 4.2 V versus Li metal reference. Furthermore, LCO possess a relatively high theoretical capacity of 270 mAhg^{-1} for cathode materials. The disadvantages of using LiCoO_2 are safety reasons, difficult access to cobalt resources, capacity fading at high potentials, poor rate performance, Co toxicity, and a low practical capacity of only 148 mAhg^{-1} [1,39,40]. For LiNiO_2 , capacities higher than 240 mAhg^{-1} are obtained in practice for the first cycle at an average voltage of 3.8 V [1,39]. Unfortunately, LiNiO_2 does not show a stable cycling behaviour. Therefore, one way to increase the capacity of the cathode material is to replace Co partly with the less expensive metal Ni in LiCoO_2 [9,39]. This has been successfully done by adding a third metal, i.e., Mn, to form NMC. The strong bonds of Mn to oxygen atoms stabilize the material during cycling, while Mn is not involved in the Li^+ release and uptake processes [1]. The theoretical capacity for NMC is reported to be 273 mAhg^{-1} [3]. The practical capacity of Ni-rich and of Ni-poor NMC (including $\text{LiNi}_{0.33}\text{Mn}_{0.33}\text{Co}_{0.33}\text{O}_2$ named NMC111) is over 200 mAhg^{-1} and up to 165 mAhg^{-1} , respectively [3]. Consequently, LCO and NMC are often used in commercial LIBs.

An ab-initio study on Li diffusion in Li_xCoO_2 [40] suggests Li migration via a monovacancy or divacancy mechanism. However, experiments indicate that a monovacancy mechanism is more probable [5]. Van der Ven and Ceder [40] concluded that although the results of their theoretical work were calculated for Li_xCoO_2 , the same conclusions are likely to be valid for other NMC layered materials. Consequently, the Li diffusion in LCO should behave similarly to that in NMC111, as also experimentally shown [7].

The temperature dependence of the Li tracer diffusivities in pressed and sintered LCO [5,7] and NMC111 [41] pellets was determined using SIMS experiments. The diffu-

sivities were determined over the temperature range of 100–500 °C. The diffusivities of NMC111 and LCO are the same within experimental error limits (Figure 1). An activation enthalpy of $\Delta H = (0.85 \pm 0.03)$ eV and a pre-exponential factor (D_0) of $\ln(D_0/m^2 s^{-1}) = -18.42 \pm 0.74$ was determined for NMC111. A pre-exponential factor of $\ln(D_0/m^2 s^{-1}) = -20.96 \pm 1.4$ and a activation enthalpy of $\Delta H = (0.75 \pm 0.03)$ eV was found for LCO. Figure 1 shows diffusivities of LCO extrapolated to room temperature according to the Arrhenius law.

$$D = D_0 \cdot \exp(-\Delta H/kT) \quad (1)$$

In this equation, D is the diffusion coefficient, D_0 is the pre-exponential factor, k is the Boltzmann constant and T is the temperature. Extrapolation from higher temperatures represents a possibility to obtain the diffusivity at room temperature, under the assumption that the diffusion mechanism remains unchanged. This has been demonstrated experimentally for the case of NMC111 [9].

Figure 1 shows that the Li tracer diffusivity of LCO is expected to be by extrapolation even below $10^{-22} m^2 s^{-1}$ at room temperature. Such a low diffusivity may need a considerable long annealing time in the order of years in form of storage at room temperature to be measurable by SIMS. Such a long-time experiment was not realized in the case of LCO due to time limitations, but for the case of NMC111 [9]. The exact Li tracer diffusivity was determined to be $(4.7 \pm 1.9) \times 10^{-23} m^2 s^{-1}$, which is indicated by a blue dot in Figure 1. This is a low diffusivity, but in agreement with the value extrapolated from the diffusivities at higher temperatures. This suggests that the extrapolation is a valid assumption for NMC111, which is likely also applicable for LCO. The error range of Li tracer diffusivities in NMC111 extrapolated to room temperature is between $3 \times 10^{-23} m^2 s^{-1}$ and $8 \times 10^{-23} m^2 s^{-1}$, taking into account the measured error in activation energy and pre-exponential factor. In the same way extrapolated Li tracer diffusivities between $1 \times 10^{-22} m^2 s^{-1}$ and $3 \times 10^{-22} m^2 s^{-1}$ are found for LCO. The observed diffusivities for LCO are only marginally larger, which may be attributed to experimental error. Consequently, diffusivities varying only an order of magnitude can be estimated at room temperature for LCO due to experimental error and extrapolation. This should also be a reasonable approximation for the comparison of diffusivities determined by different methods and obtained from materials produced by different techniques.

The objective of the present study is to provide an improved understanding of Li diffusion in LCO at room temperature. To this end, the chemical diffusivity will be measured in the same LCO material where Li tracer diffusivity was previously determined using SIMS (Figure 1). Chemical diffusivities are measured in pressed and sintered LCO pellets free of additives for $x \approx 1$, employing electrochemically based techniques (EIS, PITT). These methods will be applied in a way that the Li content in the LCO pellet is unmodified to a significant extent. This approach includes the assessment of various models used to determine Li chemical diffusivities in LCO. This paper is structured as follows: The following section provides a description of the materials under study and the measurement techniques employed. The third section is dedicated to the presentation of the data obtained from EIS and PITT. The fourth section comprises a critical evaluation of the results, which are compared to the diffusivities obtained from SIMS depth profiling experiments. The last section summarises these results.

2. Materials and Methods

The procedure for preparing and characterizing the sintered LCO samples was described in detail in reference [5]. First, commercial LCO powders (Sigma Aldrich, Taufkirchen, Germany) were high-energy ball milled. Afterwards, cylindrical bulk samples with 12 mm diameter were produced by uniaxial pressing at 100 MPa. The pellets were then subjected to a 24 h sintering process at 800 °C in air. The results of the inductively coupled plasma-optical emission spectroscopy (ICP-OES) (Analytik Jena PlasmaQuant PQ 9000 Elite, Jena, Germany) analysis indicated that the relative element concentrations are Li (24.64 ± 0.13) at.%, Co (24.94 ± 0.21) at.%, and O (50.42 ± 0.34) at.%. This gives a lithium-to-metal ratio

of $x = 0.99 \pm 0.01$ [5], which is identical within error limits to the value of 1. Therefore, a relative Li content of $x = 1$ is assigned to the fully lithiated sintered LCO pellets. Scanning electron microscopy (ZEISS Evo 15, Oberkochen, Germany) revealed that the pellet is composed of interconnected fused LCO clusters of about 3 μm diameter. X-ray diffraction (XRD) measurements (Bruker D8 Discover, Karlsruhe, Germany) revealed polycrystalline LCO with grain size of about 70 nm.

The EIS and PITT measurements were conducted using a custom-built three-electrode electrochemical cell. The electrolyte was propylene carbonate (PC, Sigma Aldrich, Taufkirchen, Germany, anhydrous, 99.7%) with 1 M lithium perchlorate (Sigma Aldrich, Taufkirchen, Germany, battery grade). The assembly and disassembly of the cell was done within a glove box containing argon gas (MBraun, Garching bei München, Germany), with a concentration of oxygen and water vapour of less than 1 ppm.

The current collector of the LCO electrode, which is the working electrode designated as “we”, is composed of a polished nickel disk with 1 mm in thickness and 14 mm in diameter. The LCO pellet with a thickness of 250 μm was fixed to the nickel disk by conductive agents. The counter and reference electrodes were lithium plates with a thickness of 1.5 mm and a purity of 99.9%, obtained from Alfa Aesar (Kandel, Germany). All reported LCO potentials (E_{we}) are referenced to the Li metal reference electrode. The LCO electrode was then inserted into the electrolyte-filled electrochemical cell. The process of Li^+ extraction (delithiation) from the LCO electrode is equivalent to cell charging. The electrochemical studies were conducted on a Biologic SP150 potentiostat using EC-lab software version V11.43 (Biologic, Seyssinet-Pariset, France).

Potentiostatic EIS was carried out with an amplitude of 10 mV. This study focuses on ionic diffusion, which is slow at room temperature. Consequently, the mass transfer impedance response manifests in the extremely low frequency range, and EIS was measured down to 1 mHz with an acquisition time of 7 h per spectrum.

PITT measurements were performed down to low Li^+ current densities over long time intervals as required for PITT analysis [9]. Further discussion of PITT is given in detail in reference [9]. The measurements were done at room temperature.

3. Results

3.1. Determination of the Chemical Diffusivity with EIS

An EIS spectrum measured at an open circuit voltage (OCV) of 1.4 V corresponding to the state right after sample preparation is plotted in Figure 2a and of 3.51 V after slight delithiation in Figure 2b.

The analysis of EIS data typically employs the use of equivalent circuits [9,13,14]. The data obtained in the present study can be accurately represented by the equivalent circuit schematised in Figure 2, which is given by the following expression $(R1 + Q2/R2 + Q3/(R3 + Ma5))$. This circuit represents a physically plausible model that provides a comprehensive description of the observed phenomena. The resistance $R1$ is ascribed to the cable, current collector, and electrolyte resistance. The constant phase element (CPE) $Q2$ and the resistor $R2$ can be attributed to the electrochemical double layer formed at the surface of the LCO electrode. The CPE $Q3$ and the resistor $R3$ can be attributed to the charge transfer process occurring at the LCO electrode. A linear modified restricted diffusion element ($Ma5$) is used for the simulation of the Li diffusion process in the LCO electrode.

It should be noted that direct diffusion at the interface may occur from the electrochemical double-layer, which tends to establish equilibrium between the electrochemical potentials of the electrolyte and electrode through a dynamic process. In that case, an additional Warburg element has to be connected in series with $R2$ and in parallel with $Q2$. However, this is omitted here due to the general requirement of EIS data fitting to restrict the number of elements in the equivalent circuit and to reduce the number of fitting parameters as much as possible.

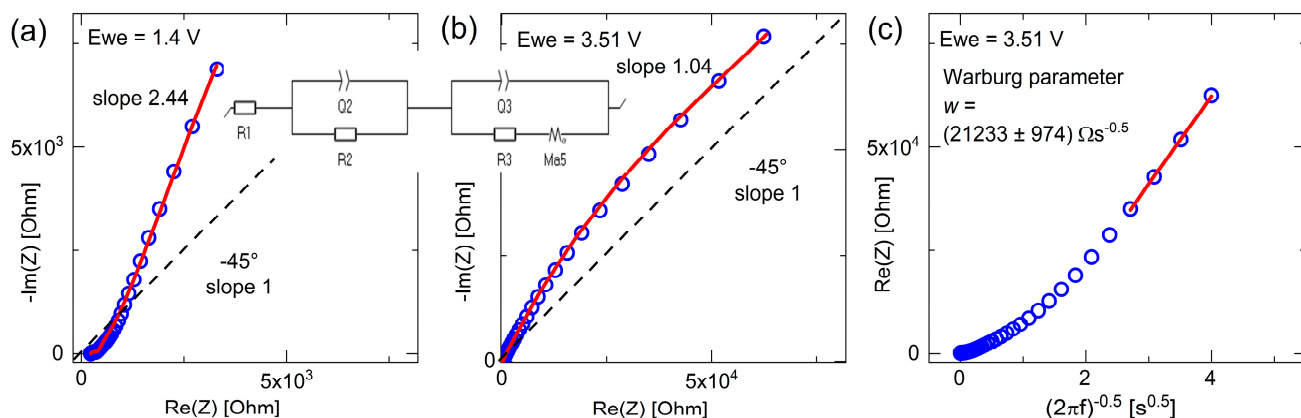


Figure 2. Results of EIS measurements on the LCO electrode marked with blue circles. The Nyquist plots were measured at (a) 1.40 V and (b) 3.51 V, respectively. The fits (red curves) were obtained using the equivalent electrical circuit $[R1 + Q2/R2 + Q3/(R3 + Ma5)]$ schematised in (a,b). The dotted line represents the behavior of a Warburg impedance. (c) Diffusion-based analysis of the EIS data from (b) by plotting the real part of the impedance as a function of the reciprocal square of the frequency.

The CPE is dependent on two parameters, Q and the exponent a . The diffusion element $Ma5$ is dependent on three parameters, $Rd5$, $a5$, and $t5$. $Rd5$ represents the resistance associated with modified restricted linear diffusion, $a5$ is an exponent, and $t5$ denotes the diffusion time constant (for further details, please see reference [9] and references therein). The diffusivity is directly related to $t5$ by the equation $D = L^2(2 t5)^{-1}$, where L is the thickness of the region where the restricted diffusion takes place. The fit to the measured data was performed using the randomized simplex method with 5000 iterations, and the following values were obtained with regard to Figure 2a: $R1 = 226 \Omega$, $R2 = 208 \Omega$, $Q2 = 153 \times 10^{-6} \text{ Fs}^{-0.5}$, $a2 = 0.5$, $R3 = 0 \Omega$, $Q3 = 500 \times 10^{-6} \text{ Fs}^{-0.1}$, $a3 = 0.9$, $Rd5 = 2300 \Omega$, $a5 = 0.73$, and $t5 = 2.1 \text{ s}$. In the case of Figure 2b, we get $R1 = 223 \Omega$, $R2 = 428 \Omega$, $Q2 = 301 \times 10^{-6} \text{ Fs}^{-0.1}$, $a2 = 0.96$, $R3 = 89,100 \Omega$, and $Q3 = 60 \times 10^{-6} \text{ Fs}^{-0.25}$, $a3 = 0.75$, $Rd5 = 831853 \Omega$, $a5 = 0.46$, and $t5 = 8943 \text{ s}$. The value of $a2 = 0.96$ is here near unity, which is indicative for an ideal electrochemical double layer capacity, in contrast to that at 1.4 V. This demonstrates that the double layer is more developed at 3.5 V than at 1.4 V. Further differences are observed in the charge transfer resistance $R3$ and the values of the diffusion element, particularly in $Rd5$ and $t5$. The calculated Li diffusivities from $t5$, considering the entire pellet thickness of $L = 250 \mu\text{m}$, yield $D(1.4 \text{ V}) = 1.6 \times 10^{-9} \text{ m}^2 \text{ s}^{-1}$ and $D(3.51 \text{ V}) = 4 \times 10^{-12} \text{ m}^2 \text{ s}^{-1}$. These diffusivities are relatively high.

It is important to note that, as discussed in detail in reference [9] and the supporting information of that reference, the methodology to obtain results from EIS data by performing fittings with equivalent circuits is ambiguous [9,13]. This is because although different equivalent circuits can produce a similar good fits to the measured EIS data, they may give different results. Furthermore, it should be noted that the precise thickness of the region where the Li diffusion occurs is currently unknown. Consequently, in the present study, an older, less frequently employed, but robust method of diffusivity determination from EIS measurements independent of film thickness is also employed, as discussed in detail in reference [9].

In the low-frequency range, the measured impedance is defined by a linear relationship with a slope of $|d(\text{Im}Z)/d(\text{Re}Z)| = 2.44$ in the Nyquist plot of Figure 2a. In reference [9] it was shown that for such slopes the Li diffusivity in the pellet cannot be determined unambiguously. This is different for slopes approaching the value 1, which is the case for the EIS spectra obtained at 3.51 V (Figure 2b). In such cases, a reasonable Li diffusivity can be obtained using the concept of the Warburg impedance [9] as shown in Figure 2c.

In a plot of $\text{Re}(Z)$ versus $f^{-0.5}$, where f is the frequency, the Warburg impedance produces a straight line. The diffusivity is determined from the slope of the line in Figure 2c according to [9]

$$D = \left(\frac{R \cdot T}{(\sqrt{2}) \cdot n^2 \cdot F^2 \cdot a_e \cdot c} \cdot \frac{1}{c} \cdot \frac{1}{w} \right)^2 \quad (2)$$

In this equation, R represents the universal gas constant, T denotes a temperature of 300 K, a_e signifies the lithiated area, n is the valence number, F is the Faraday constant, and c is the Li^+ concentration, which is expressed as a function of the molar mass (M_{LCO}) and the mass density ($\rho_{\text{LCO}} = 4.8 \text{ g cm}^{-3}$) of LCO. The SOC is defined as the percentage of Li ions that are present in the LCO material. The SOC is equal to 1 when the material is fully lithiated. The Warburg parameter (w) is a measure of Li ion diffusion through the material. It is calculated by fitting a linear function to the data in Figure 2c and determining the slope.

In the case of high frequencies and high diffusivities, or in the context of thick films (i.e., in the absence of any restrictions on diffusion), the following equation can be applied [9]:

$$D = \left(\frac{\frac{V_M}{SOC}}{(\sqrt{2}) \cdot n \cdot F \cdot a_e} \cdot \frac{dE}{dy} \cdot \frac{1}{w} \right)^2 = \left(\frac{1}{(\sqrt{2}) \cdot n \cdot F \cdot a_e} \cdot \frac{dE}{dy} \cdot \frac{1}{c} \cdot \frac{1}{w} \right)^2 \quad (3)$$

The slope of the open circuit voltage versus composition curve represented by dE/dy is calculated using the Li content y . The mole volume of Li in LCO is calculated to $V_M = (M_{\text{LCO}}/\rho_{\text{LCO}})$. Consequently, the ratio of V_M to SOC is equal to $1/c$. In the present study, the dE/dy value is determined by examining the relationship between the SOC and the electrode potential in LCO (Figure 3d).

The fit in Figure 2c gives a Warburg parameter of $(21233 \pm 974) \Omega \text{s}^{-0.5}$. Diffusivities of $(5.5 \pm 3) \times 10^{-24} \text{ m}^2 \text{s}^{-1}$ and $(3.4 \pm 2) \times 10^{-25} \text{ m}^2 \text{s}^{-1}$ are obtained using Equations (2) and (3), respectively. These are low values compared to the results of equivalent circuit fitting. The Li diffusivity determined by Equation (3) at the potential of 3.51 V for NMC111 is $(1.6 \pm 0.6) \times 10^{-12} \text{ m}^2 \text{s}^{-1}$ which is thirteen orders of magnitude higher than in this work measured for LCO. This large discrepancy may be due to different SOCs of the two materials. For LCO and NMC111, the SOC at a potential of 3.51 V is about 99.95% and 98.00%, respectively. This means that at 3.51 V, 40 times more Li is extracted from NMC111 than from LCO. Reference [9] has shown for NMC111 that there is an exponential increase in the Li diffusivity with the amount of Li extracted close to 3.5 V. The SOC of 99.95% obtained for LCO at 3.51 V is obtained for NMC111 at a potential of 2.8 V. The literature also shows that the onset of Li extraction from LCO [4] occurs at higher potentials than from NMC111 [9]. For NMC111, delithiation starts at 3.5 V [9], whereas for LCO, the delithiation plateau in the Ewe vs. Li composition curve does not start before 3.9 V [4]. Since the Li diffusivity increases sharply with decreasing Li content at the onset of charging in both LCO [4] and NMC111 [9], the higher Li content in LCO at 3.51 V compared to the lower Li content in NMC111 at 3.51 V results in a lower Li diffusivity in LCO at 3.51 V, closer to the completely lithiated state.

3.2. Determination of the Chemical Diffusivity and of the Thermodynamic Factor with PITT

PITT is a potential-step chronoamperometric method that measures the current response versus time as successive small voltage steps are applied. It is a widely used method to determine diffusion coefficients in electrochemical materials, especially Li diffusion in LIBs [9]. The voltage steps and current response of typical measured PITT curves are shown in Figures 3a and 3b, respectively. Figure 3c illustrates the plot of the Li^+ charge extracted from the LCO electrode during each voltage step as a function of potential. It can be observed that the extracted charge is in the range of $\mu\text{Ah cm}^{-2}$, which is a low value in comparison to the total Li^+ content of the LCO electrode, which is calculated to

be $\approx 30,000 \mu\text{Ahcm}^{-2}$. The low amount of extracted charge in Figure 3c fulfills the general requirement of diffusivity determination via the pulse method [9]. The cumulative Li⁺ charge, expressed in terms of the SOC of the LCO electrode at each potential (after each PITT step), is plotted in Figure 3d.

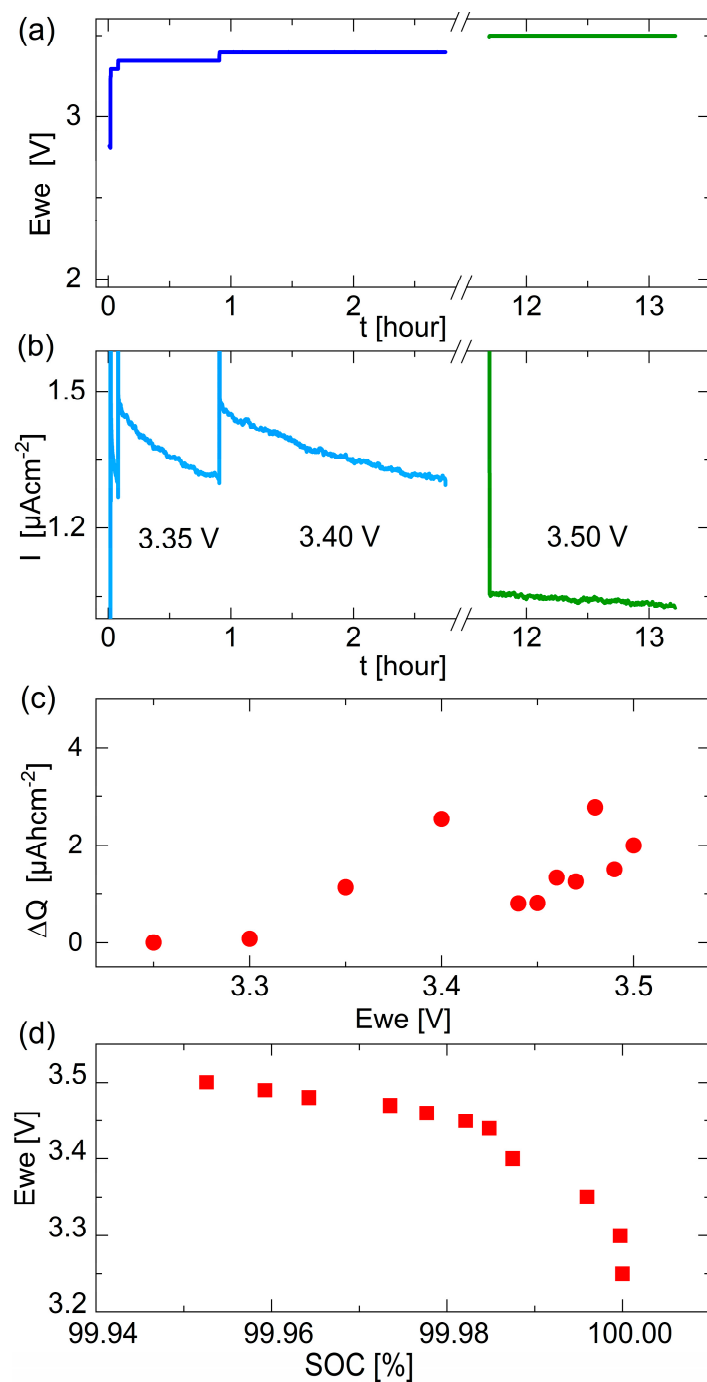


Figure 3. Results of PITT measurements. (a) Voltage steps between 3.2 and 3.4 (blue lines) and at 3.5 V (green line) versus time. (b) Current response between 3.2 and 3.4 (blue lines) and at 3.5 V (green line) versus time. (c) Charge (red circles) extracted during each voltage step (d) The SOC (red squares) present in the electrode during the subsequent voltage step that is indicative for the degree of lithiation (SOC = 100% represents the fully lithiated state). Voltage steps of 50 mV were used up to 3.4 V and 10 mV steps above.

Figure 4 illustrates the measured PITT data at 3.50 V, presented in a series of distinct plots. The Li diffusivity can be calculated from a plot of current versus the square root of the inverse of time (I vs. $t^{-0.5}$, Figure 4b) and from a logarithmic plot of current ($\ln(I)$ vs. t , Figure 4c). It should be noted that the analysis of PITT data depends on the dimensions of the electrode, particularly the thickness of the electrode or the radius of the particles present in the case of powders or agglomerates. In the Equation (4), L represents the characteristic length of the electrode material. The LCO electrode used in the present study is composed of approximately 3 μm clusters of sintered particles with grain sizes of approximately 70 nm. There are no well-separated particles, but rather a bulk material. Consequently, we first employ the LCO electrode thickness ($L = 250 \mu\text{m}$) for PITT analysis.

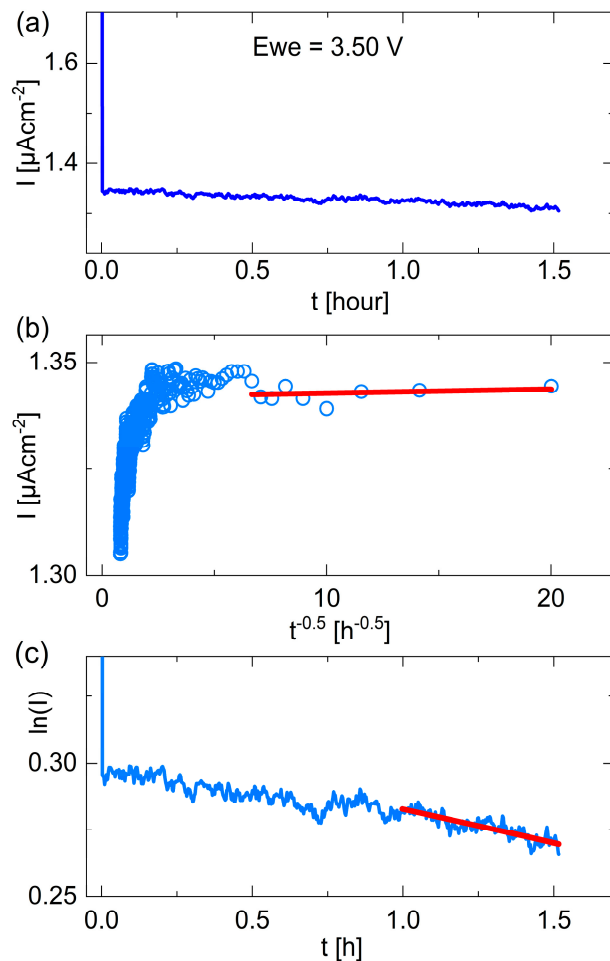


Figure 4. (a–c) The current response (blue curves) as a function of time during a typical PITT voltage step recorded at an LCO electrode potential of 3.50 V on different scales. The fits using Equations (4) and (6) are represented in (b,c) as the red line.

For short times (Figure 4b), the following equation is used to determine diffusivities by PITT [9]

$$I = a_{short} + b_{short} \cdot \frac{1}{\sqrt{t}} \text{ with } a_{short} = 0 \implies D_{short} = \frac{\pi \cdot L^2}{Q^2} \cdot b_{short}^2 \quad (4)$$

where D_{short} is the corresponding diffusivity and Q is the charge extracted or inserted during the PITT step. Furthermore, b_{short} is the slope (red line in Figure 4b).

In addition to the requirement $a_{short} = 0$, the time interval Δt_{short} , from which the diffusivity is determined via Equation (4), have to satisfy the following inequality [9]

$$\Delta t_{short} < 0.14 \cdot t_D = 0.14 \cdot \frac{L^2}{2 \cdot D_{short}} = 0.14 \cdot \frac{Q^2}{2 \cdot \pi \cdot b_{short}^2} \quad (5)$$

where $t_D = L^2(2D_{short})^{-1}$ is the time required for Li to diffuse across the characteristic length of the material under investigation (e.g., electrode thickness L). The last term shows that the requirement (5) is formally independent of the characteristic length of the electrode material.

In the case of long-term domain PITT (Figure 4c), the following equation is employed in order to ascertain the diffusivities [9].

$$\ln(I) = a + b \cdot t \implies D_{a-long} = \frac{L^2}{2 \cdot Q} \cdot e^a, D_{b-long} = \frac{4 \cdot L^2}{\pi^2} \cdot b \quad (6)$$

where D_{a-long} and D_{b-long} are the diffusivities obtained in this analysis (Figure 4c), D_{a-long} from the intercept of the y-axis (parameter a) and D_{b-long} from the slope (parameter b). The time interval Δt_{long} (necessary for diffusivity determination) has to fulfill the following conditions [9].

$$\Delta t_{a-long} > 0.14 \cdot t_D = 0.14 \cdot \frac{L^2}{2 \cdot D_{a-long}} = 0.14 \cdot \frac{Q}{\pi \cdot e^a} \quad (7)$$

$$\Delta t_{b-long} > 0.14 \cdot t_D = 0.14 \cdot \frac{L^2}{2 \cdot D_{b-long}} = 0.14 \cdot \frac{\pi^2}{8 \cdot b} \quad (8)$$

The last term of Equations (7) and (8) shows that the requirements (7) and (8) are independent of the characteristic length of the electrode material (L).

As obvious, linear segments were detected in the I vs. $t^{-0.5}$ (Figure 4b) and $\ln(I)$ vs. t (Figure 4c) plots. These were fitted with Equations (4) and (6), respectively. Figure 5a shows the diffusivities D_{short} , D_{a-long} and D_{b-long} from the PITT, and also those from EIS measurements.

EIS and PITT give chemical diffusivities (D_{chem}). In case of the electronic conductivity is higher than ion conductivity they are correlated to the tracer diffusivities (D_{tracer}), (e.g., obtained by SIMS) by the thermodynamic factor (TF) [4,34] according to Equation (9)

$$D^{PITT,GITT,EIS} = D_{chem} = TF \cdot D_{tracer} \quad (9)$$

PITT measurements [4,34] can be used to determine the TF according to

$$TF = \frac{F}{R \cdot T} \cdot \frac{Q}{\Delta Q} \cdot \Delta E_{we} \quad (10)$$

In this equation, F represents the Faraday constant, R is the universal gas constant, T = 300 K is the temperature, Q is the total number of Li^+ ions in the LCO electrode at the current SOC, and ΔQ is the Li^+ charge extracted from the LCO electrode during a potential step. Additionally, ΔE_{we} is the potential step. The thermodynamic factor calculated to Equation (10) is plotted in Figure 6a.

The chemical and tracer diffusivities plotted in Figures 5 and 6 will be further discussed in the next section by taken into account constraints and corrective considerations. Here, we briefly mention that the chemical diffusivities in Figure 5a decrease with higher LCO potentials (lower SOC, see Figure 3d). The trend of diffusivity decrease is not only observed for PITT experiments, but it can also be evidenced from the diffusivities obtained by fitting the EIS data with equivalent circuits (the black crosses and the violet stars in Figure 5). On the other hand, the tracer diffusivities (Figure 6b) are almost constant versus the SOC with the exception of some PITT data very close to 100% SOC. However, an unsatisfying result of Figures 5 and 6 is the high scatter of the diffusivity data over more than 15 orders of magnitudes, a result which will be discussed in more detail in the next section.

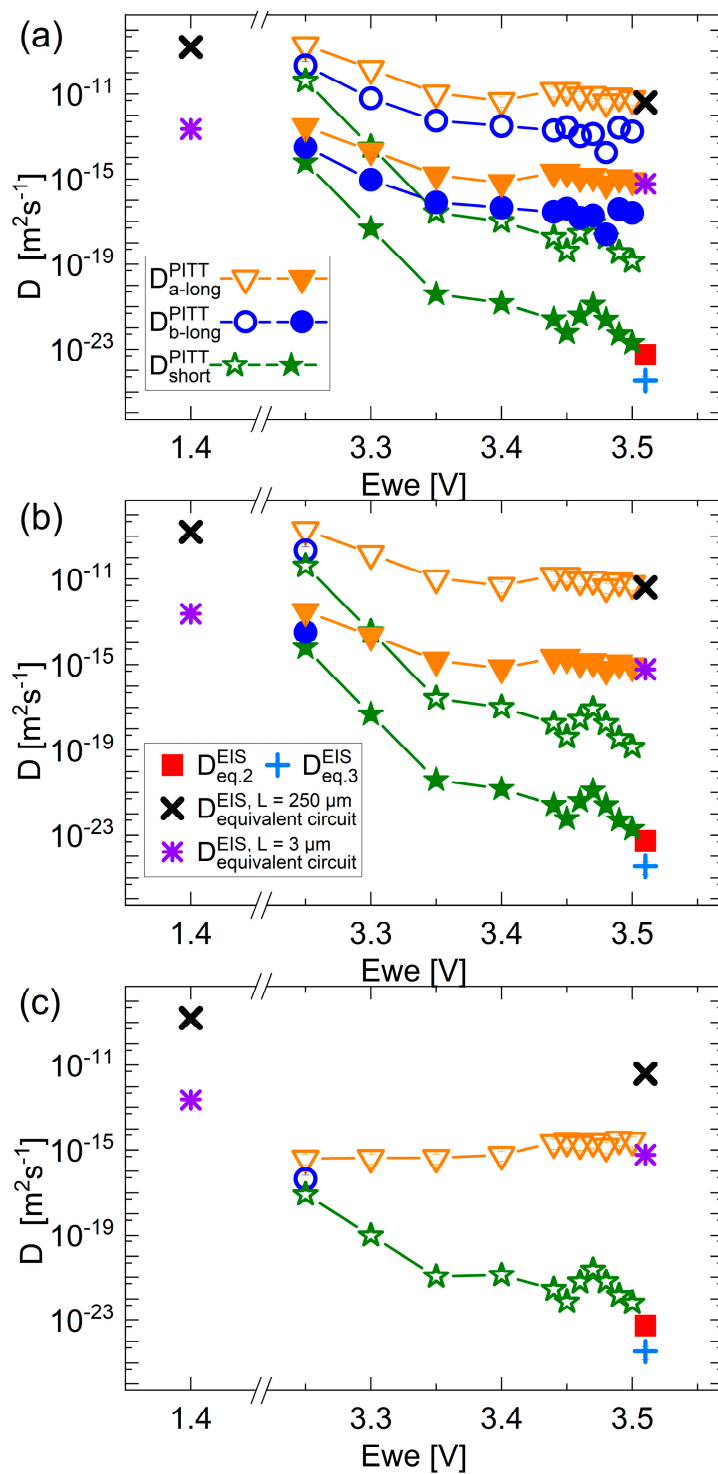


Figure 5. (a–c) Chemical diffusivities versus the LCO electrode potential: (a) As obtained from PITT and EIS. (b) All diffusivities that do not satisfy the requirements (4), (5), (7) and (8) are excluded from the plot. (c) The corrected Li diffusivities (D^{PITT}) were calculated under consideration of a moving phase boundary mechanism during delithiation by Equation (11). D^{PITT} values shown with unfilled and solid symbols correspond to values calculated using $L = 250 \mu m$ and $3 \mu m$, respectively. The black crosses and the violet stars correspond to the diffusivities obtained from equivalent circuit fitting of EIS data measured at an LCO potential of 1.4 V and 3.51 V, using $L = 250 \mu m$ and $3 \mu m$, respectively.

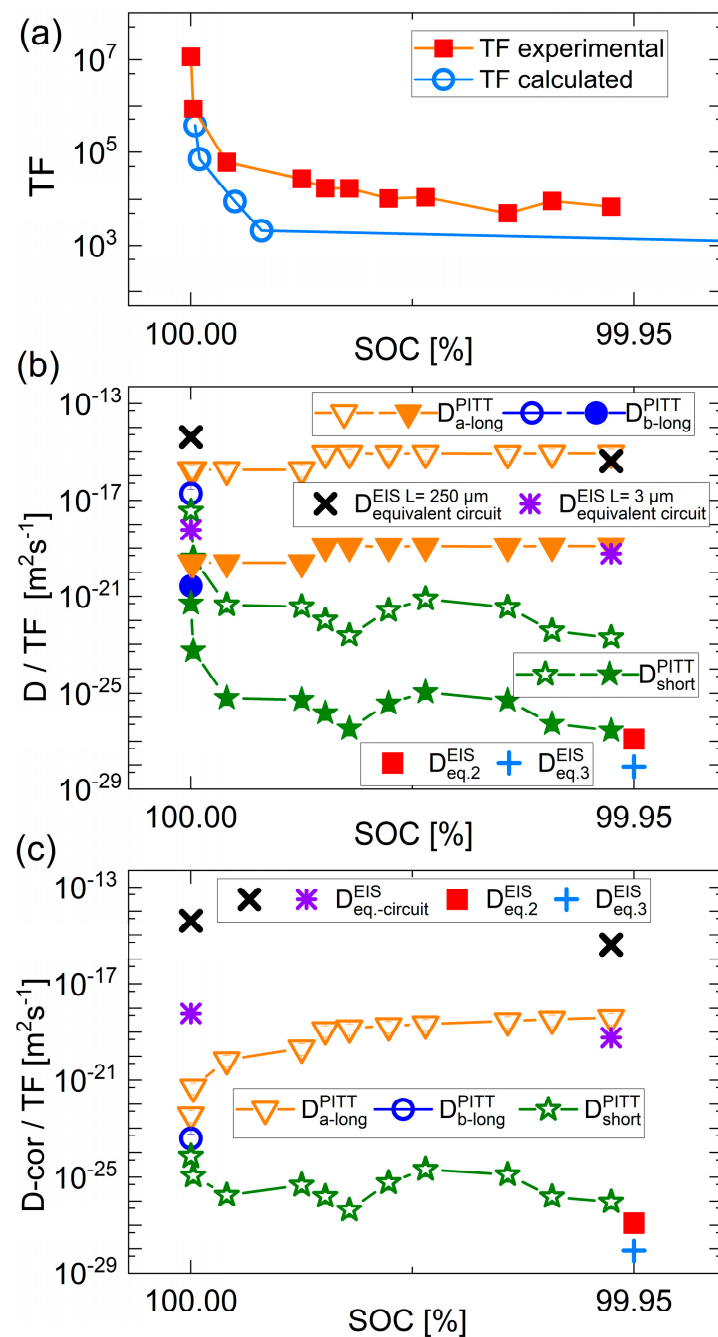


Figure 6. (a) The thermodynamic factor (TF) plotted as a function of SOC, as determined from PITT experiments on LCO. Additionally, the TF is theoretically obtained from first-principle calculations on LCO, as presented in the literature [40]. (b) The SOC dependence of the Li tracer diffusivity in LCO. (c) The corrected Li diffusivities, taking into account a presumed two phase delithiation process. D^{PITT} values shown with unfilled and solid symbols correspond to values calculated using $L = 250 \mu m$ and $3 \mu m$, respectively. D^{EIS} values shown with black crosses and violet stars correspond to diffusivities obtained from equivalent circuit fitting using $L = 250 \mu m$ and $3 \mu m$, respectively.

4. Discussion

First, note that the diffusivities under discussion represent average values due to the anisotropy of the LCO structure and pellet morphology. It should be noted that the formation of an equilibrium between the electrochemical potentials of the electrolyte and electrode may be associated with a diffusion process from the electrochemical double-layer capacitor. Our results indicate that Li-ion diffusion may occur in regions with a reduced

thickness, probably also in proximity to the electrochemical double layer. This might be associated with the tunneling of electrons that neutralize the Li ions in the electrolyte, thereby reducing the influence of coulombic forces on short-range diffusion. Subsequently, the neutral Li atom may lose an electron while migrating within the cathode.

The diffusivities determined from the EIS measurements with the help of equivalent circuit fitting, and those according to Equations (2) and (3) are shown in Figure 5a–c as black crosses, violet stars, red-filled squares and blue plus signs, respectively. Figure 5a also gives the diffusivities obtained from PITT by the three distinct methods, using Equations (4) and (6). The PITT data indicate a similar qualitative behaviour as a function of potential. As previously mentioned, the potential increases during delithiation and the diffusivities decrease. In quantitative terms, the diffusivities $D_{a\text{-long}}^{\text{PITT}}$ and $D_{b\text{-long}}^{\text{PITT}}$, obtained by applying Equation (6) to the long-time domain of the PITT signal, are more similar to each other than to $D_{\text{short}}^{\text{PITT}}$. These values are up to seven orders of magnitude higher than those obtained from the short-time domain of the PITT signal ($D_{\text{short}}^{\text{PITT}}$). The considerable discrepancy between the diffusivities obtained from the short-time and long-time domains remains unexplained, underlining the inherent limitations of deriving reliable diffusivities from electrochemical methods with different models. An adjustment can be made when these diffusivities are examined for their validity in accordance with the conditions given in Equations (4), (5), (7) and (8). Data points that do not satisfy these conditions are excluded, and the remaining data are presented in Figure 5b. Further details can be found in reference [9]. $D_{b\text{-long}}^{\text{PITT}}$ does not fulfill condition (8) for nearly all potentials and is not considered further (Figure 5b). The discrepancy between the values of $D_{a\text{-long}}^{\text{PITT}}$ and $D_{\text{short}}^{\text{PITT}}$ persists.

A further issue arises when the diffusivities obtained from the EIS measurements are compared to those obtained by PITT (Figure 5). The diffusivities determined from the EIS measurements by Equations (2) or (3), are found to be lower than those obtained from the PITT experiments. This suggests that either the Equations (2)–(4) and (6) or the values of the parameters used in those formulas are incorrect. The diffusivities extracted using the equivalent circuit on EIS data are in agreement to the $D_{\text{long}}^{\text{PITT}}$ data.

With respect to the parameters used in the equations, two possible errors may exist: the characteristic length (L) inserted in the PITT Formulas (4) and (6) and the Li concentration (c) in the EIS Formulas (2) and (3). Concerning the characteristic length L , it should be noted that this quantity may differ from the overall thickness of the sintered LCO pellet of about 250 μm . Due to the low Li diffusivities present, the Li^+ current delivered by the PITT step on the electrode surface has insufficient time to cross the whole thickness of the LCO pellet during the relevant time scale. Since the quantity L is a variable in the PITT Formulas (4) and (6), it is not possible to derive the true diffusion length during the PITT experiment. The much lower diffusivity determined by EIS using Equations (2) or (3) (Figure 5b) indicates that the value of L to be used in the PITT Equations (4) and (6) has to be much smaller than 250 μm .

Using the assumption that the characteristic length L is the cluster size of 3 μm as visible by SEM measurements, instead, we recalculated the D^{PITT} values correspondingly. This gives the diffusivities shown in Figure 5 with full symbols. However, the $D_{\text{long}}^{\text{PITT}}$ values are still higher than those obtained from the EIS measurements using the Equations (2) and (3). On the other hand, the $D_{\text{short}}^{\text{PITT}}$ values now agree much better with that D^{EIS} values (Figure 5a,b).

An alternative procedure is to consider a specific delithiation mechanism at the onset of LCO charging, as has been done for sintered NMC111 pellets in reference [9]. Assuming that a two-phase delithiation mechanism is at work during the onset of LCO charging, it is possible to calculate the thicknesses in Equations (4) and (6) using the following formula

$$L = L_0 \cdot \frac{100\% - \text{SOC}}{100\%} \quad (11)$$

where $L_0 = 250 \mu\text{m}$ is the thickness of the electrode, and the SOC is given in percentage. Since the potential remains approximately constant during the onset of charging (see, for example, Figure 2a of reference [4]), a two-phase lithiation process might be justified. A more detailed explanation can be found in the supporting information of reference [9].

Combining Equations (4) and (6) with Equation (11), the resulting corrected DPITT values are presented in Figure 5c. There is now also a good agreement between the diffusivities determined in the present study from EIS (using Equations (2) and (3)) and PITT experiments for $D_{\text{short}}^{\text{PITT}}$. As the electrode potential decreases, the corrected $D_{\text{short}}^{\text{PITT}}$ exhibit a corresponding decline, a phenomenon that is analogous to the observations made in the case of NMC111 [9]. Close to a SOC of 100%, all diffusivities obtained from PITT show approximately the same value within about an order of magnitude.

It is important to note that the assumption of a planar two-phase delithiation mechanism, as recognized in amorphous silicon thin films [35,42,43], requires experimental verification for the case of LCO. For LCO [s53,s55,s56], Lu et al. [44,45] used high-resolution transmission electron microscopy with a resolution of 0.04 nm to gain insight into the atomic structure of delithiated LCO nanoparticles. They constructed a phase diagram for the delithiation of LCO nanoparticles as a function of the LCO electrode potential and the amount of Li extracted from LCO, for instance, as a function of y in $\text{Li}_{1-y}\text{CoO}_2$ up to $y \approx 0.5$ (Figure 5 in reference [44] and Figure 6c in reference [45]). For Li extraction corresponding to y between 0.06 and 0.23, there is a two-phase situation, but not for lower values of extracted Li, which is the range of the current study. It is noteworthy that the aforementioned correction, as given in Equation (11), was not applied to the EIS results obtained with Equations (2) and (3) because they are independent of the thickness, L . We are uncertain whether to apply the correction to EIS results from equivalent circuit fitting.

The second uncertainty relates to the use of the appropriate value for the Li concentration in the EIS Formulas (2) and (3). It is unclear whether the total Li concentration of LCO should be used in these equations. The hypothesis is that not all Li ions in LCO migrate during the EIS experiment, but only a fraction of the total Li amount. The precise quantity of Li participating in the EIS measurement remains unknown. Therefore, we propose an alternative approach, where the diffusivities derived from EIS and the uncorrected PITT values are assumed to be equal at 3.5 V, allowing us to assess the Li concentration that is mobile during the EIS measurement. Assuming $D^{\text{EIS}} = D_{\text{short}}^{\text{PITT}} = 1.3 \times 10^{-19} \text{ m}^2\text{s}^{-1}$ and $2 \times 10^{-23} \text{ m}^2\text{s}^{-1}$, and $D^{\text{EIS}} = D_{\text{a-long}}^{\text{PITT}} = 6 \times 10^{-12} \text{ m}^2\text{s}^{-1}$ and $8 \times 10^{-16} \text{ m}^2\text{s}^{-1}$, for the case of $L = 250 \mu\text{m}$ and $3 \mu\text{m}$, respectively, the partial Li concentration that is mobile during the EIS experiments is determined from Equation (12), and the resulting values are listed in Table 1.

$$\frac{c_{\text{Li}}^{\text{EIS}}}{c_{\text{Li}}^{\text{total}}} = \sqrt{\frac{D_{\text{eq2,eq3}}^{\text{EIS}}}{D_{\text{short, a-long}}^{\text{PITT}}}} \quad (12)$$

Table 1. The partial Li concentrations calculated from Equation (12), which is likely to be mobile during the EIS experiments. The partial Li concentrations obtained using $L = 250 \mu\text{m}$ and $3 \mu\text{m}$ in the D^{PITT} calculation are listed in the second and third rows, respectively.

L	$D_{\text{eq2}}^{\text{EIS}}, D_{\text{short}}^{\text{PITT}}$	$D_{\text{eq2}}^{\text{EIS}}, D_{\text{a-long}}^{\text{PITT}}$	$D_{\text{eq3}}^{\text{EIS}}, D_{\text{short}}^{\text{PITT}}$	$D_{\text{eq3}}^{\text{EIS}}, D_{\text{a-long}}^{\text{PITT}}$
250 μm	$c_{\text{Li}}^{\text{EIS}} / c_{\text{Li}}^{\text{total}}$	0.6%	0.00009%	0.16%
3 μm	$c_{\text{Li}}^{\text{EIS}} / c_{\text{Li}}^{\text{total}}$	50%	0.075%	14%

The values are relatively low, ranging from 0.6% to less than 0.00003% of the total Li concentration in LCO using $L = 250 \mu\text{m}$ for PITT analysis. Using $L = 3 \mu\text{m}$, the values are, obviously, higher, reaching even 50% (Table 1). However, it is unclear which of these values are relevant.

It can be concluded that the true Li diffusivity cannot be identified in a consistent way from the widely varying diffusivities obtained by the indirect diffusion determination methods based on electrochemical measurements. To solve this problem, it is necessary to determine the Li diffusivity independently using tracer diffusion methods with SIMS depth profiling experiments for comparison.

The Li diffusivities determined via EIS and PITT represent chemical diffusivities (D_{chem}), which are different from the tracer diffusivities (D_{tracer}) by the thermodynamic factor (TF) [4,34], as illustrated by Equation (10). The TF obtained from the PITT measurements is plotted in Figure 6a. It decreases significantly with decreasing SOC, corresponding to an increasing deviation from stoichiometry. These results are in good agreement with first-principles calculations of Li diffusion in layered Li_xCoO_2 [40]. Calculations show that if x approaches a value of 1, the Li chemical potential deviates strongly from ideal behavior. The current regime exhibits a substantial amplifying effect of a slight variation in Li concentration on the chemical potential gradient, resulting in a large TF.

Equation (9) was used to calculate the tracer diffusivities from the chemical diffusivities as illustrated in Figure 6b and with consideration of the two-phase delithiation mechanism in Figure 6c. The tracer diffusivities demonstrate a relatively independent behavior with respect to the SOC, below the exact stoichiometric composition (SOC = 100%).

Figure 7 presents a comparison of Li tracer diffusivities obtained from electrochemical methods using diverse models and appropriate assumptions for diffusivity determination (i.e., varying equations and parameters) as discussed above (positions (1) to (15)). These values are compared to the tracer diffusivities obtained from SIMS depth profiling experiments (position (16)). This is undertaken in order to provide a reliable basis for the determination of correct diffusion coefficients. As previously discussed, the Li tracer diffusivities determined from electrochemically based measurements exhibit a considerable degree of scatter with values ranging between 10^{-15} and $10^{-28} \text{ m}^2\text{s}^{-1}$ (Figure 7).

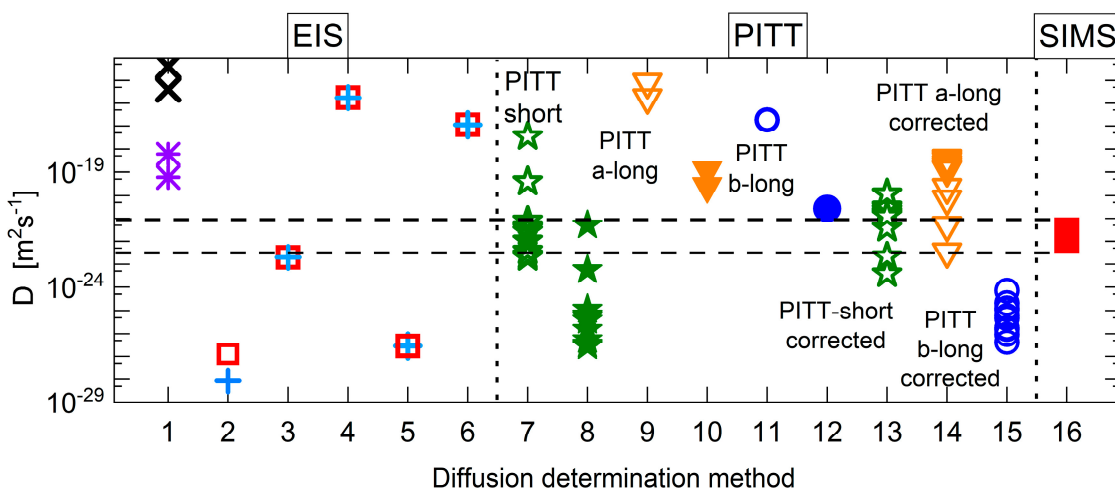


Figure 7. Li tracer diffusivities at room temperature derived from various electrochemical diffusion experiments on fully lithiated and slightly delithiated sintered LCO pellets (numbers (1) to (15)). The data at position (1) to (6) were obtained from EIS, while the data at positions (7) to (15) were obtained from PITT measurements, using different models, including different equations and different parameters. D^{PITT} values shown with unfilled and solid symbols correspond to values calculated using $L = 250 \mu\text{m}$ and $3 \mu\text{m}$, respectively. Position (16) refers to values extrapolated to room temperature from the SIMS data at higher temperatures. The diffusivity region within the two horizontal dashed lines comprises the range of diffusivities that is acceptable from the perspective of the SIMS results. For further details the reader is directed to the main text.

As previously stated in the introduction section, the extrapolation of SIMS data obtained at elevated temperatures to room temperature may be a valuable method for the

class of NMC materials, which includes LCO (Figure 1). The two horizontal dashed lines in Figure 7 indicate the range of Li tracer diffusivities that are reliable from the perspective of the SIMS result (position (16)). The initial six positions in Figure 7 pertain to the diffusivities derived from EIS measurements. The black crosses (\times) and violet stars were obtained from fitting the EIS data with an equivalent circuit (Figure 2) by using $L = 250 \mu\text{m}$ and $L = 3 \mu\text{m}$, respectively, in the diffusivity calculation. The red-filled squares and the blue plus signs indicate the data obtained by EIS, which were obtained using Equations (2) and (3), respectively. Position (2) pertains to diffusivities for the maximum concentration of mobile Li. Positions (3) and (4) refer to a partial Li concentration from the third and fourth as well as fifth and sixth columns of the second row of Table 1. Finally, the data at positions (5) and (6) refer to the partial Li concentration of the third row of Table 1. It can be observed that the EIS data at position (3) fall within the range of acceptable diffusivities, which would indicate that not all Li in the sintered LCO pellet are mobile during the EIS measurement, but only 1.6%, which is considerable low.

The diffusivities obtained from PITT (positions (7) to (15)) exhibit also a high degree of scatter. The values at the different positions are marked in the plot. The D^{PITT} values plotted with unfilled symbols (at positions (7), (9), (11), (13), (14), (15)) and solid symbols (at positions (8), (10), (12)) correspond to values calculated using $L = 250 \mu\text{m}$ and $3 \mu\text{m}$, respectively. Equation (11) was used only for the values at positions (13), (14) and (15). The SIMS results are in good agreement with some of the PITT result in positions (7), (8), (13), and (14) close to a SOC of 100%. However, the problem is that at those positions the diffusivities were determined by different approaches. This means that in a comparative study like the present one, it is not possible to determine which of the various electrochemical methods of diffusivity determination is the most appropriate.

To summarize, the determination of Li diffusivities from electrochemical-based measurements gives values spanning a range of 21 orders of magnitude also close to 100% of SOC. The application of a well-established Li selective and direct tracer diffusion method, such as SIMS depth profiling, can effectively narrow the range of diffusivities to approximately one order of magnitude. This demonstrates that to ensure greater reliability in diffusivity determination, diffusivities obtained from electrochemical-based methods should be compared to those obtained by tracer diffusion methods. Another key finding of the current study is the existence of low tracer diffusivities and large TFs prior to the onset of the electrochemical delithiation process of sintered LCO pellets, which is similar to the case of NMC111 [9].

5. Conclusions

Li tracer diffusivity, Li chemical diffusivity, and thermodynamic factor were determined through experiments on pressed and sintered LCO bulk electrodes at room temperature. The material was free of binders and conductive agents in order to enable a measurement of the intrinsic Li diffusivity. The measurements were conducted using PITT and EIS on samples that were fully lithiated and only slightly delithiated (SOC > 99.95%). The chemical diffusivity was determined from EIS experiments to range between $1.5 \times 10^{-9} \text{ m}^2\text{s}^{-1}$ and $3.4 \times 10^{-25} \text{ m}^2\text{s}^{-1}$, depending on the applied diffusivity determination formula. The chemical diffusivities obtained from PITT also span a large range, between $10^{-9} \text{ m}^2\text{s}^{-1}$ and $10^{-23} \text{ m}^2\text{s}^{-1}$. The values depend on the applied formula of diffusivity determination and on the so-called characteristic length of the electrode material, to which diffusion is restricted during the PITT experiment, e.g., considering the whole thickness of the LCO pellet ($\approx 250 \mu\text{m}$) or only the size of $\approx 3 \mu\text{m}$ of the clusters of interconnected LCO particles of the LCO pellet. The agreement between the diffusivities obtained by PITT and those obtained by EIS (which were obtained without the need of a characteristic diffusion length) is improved by two factors: (i) a presumed two-phase delithiation mechanism at the onset of LCO charging for the PITT experiments, and (ii) a reduced mobile Li ion concentration for the EIS experiments. It must be acknowledged that both assumptions have

yet to be validated through experiments. It is therefore imperative that future experiments are designed to address these shortcomings.

In order to identify the most reliable Li diffusivities, a comprehensive analysis was carried out on electrochemically determined values using diverse suited models and assumptions. These values were then compared with the diffusivities derived from the established ${}^6\text{Li}$ tracer diffusion experiments by SIMS. A comparison was done between the chemical diffusivities obtained by PITT and EIS and the Li tracer diffusivities estimated from SIMS experiments, with the thermodynamic factor measured by PITT. The Li tracer diffusivities obtained from PITT and EIS fall within the range of 10^{-15} and $10^{-28} \text{ m}^2\text{s}^{-1}$. Extrapolation of tracer diffusivities measured by SIMS to room temperature yielded a value between $1 \times 10^{-22} \text{ m}^2\text{s}^{-1}$ and $3 \times 10^{-22} \text{ m}^2\text{s}^{-1}$, confirming the indication of a very low Li tracer diffusivity. Therefore, the SIMS results help to restrict the range of possible Li tracer diffusivities determined electrochemically to a narrow band within one order of magnitude around $10^{-22} \text{ m}^2\text{s}^{-1}$. A further significant outcome of the present study is the identification of low diffusivities and elevated thermodynamic factors at room temperature preceding the initiation of electrochemical delithiation in sintered LCO pellets, exhibiting a similar trend to that observed in the other layered cathode material, $\text{LiNi}_{0.33}\text{Mn}_{0.33}\text{Co}_{0.33}\text{O}_2$.

Author Contributions: Conceptualization, H.S. and E.H.; methodology, H.S. and E.H.; validation, H.S. and E.H.; formal analysis, E.H.; investigation, E.H.; resources, H.S.; data curation, H.S. and E.H.; writing—original draft preparation, E.H.; writing—review and editing, H.S. and E.H.; visualization, E.H.; supervision, H.S.; project administration, H.S.; funding acquisition, H.S. All authors have read and agreed to the published version of the manuscript.

Funding: This research was funded by the Deutsche Forschungsgemeinschaft (DFG, German Research Foundation) under the contract SCHM 1569/33-2 (413672097). The financial support is gratefully acknowledged.

Data Availability Statement: Dataset available on request from the authors.

Acknowledgments: We thank Daniel Uxa for preparing the sintered LCO pellet and Gerrit Zander (TU Clausthal) for determining the stoichiometry of the LCO pellet using ICP-OES.

Conflicts of Interest: The authors declare no conflicts of interest.

References

- Booth, S.G.; Nedoma, A.J.; Anthonisamy, N.N.; Baker, P.J.; Boston, R.; Bronstein, H.; Clarke, S.J.; Cussen, E.J.; Daramalla, V.; De Volder, M.; et al. Perspectives for next generation lithium-ion battery cathode materials. *APL Mater.* **2021**, *9*, 109201. [[CrossRef](#)]
- Hüger, E.; Riedel, L.; Zhu, J.; Stahn, J.; Heijmans, P.; Schmidt, H. Lithium niobate for fast cycling in Li-ion batteries: Review and new experimental data. *Batteries* **2023**, *9*, 244. [[CrossRef](#)]
- Tang, Z.; Feng, D.; Xu, Y.; Chen, L.; Zhang, X.; Ma, Q. Perspectives for next generation lithium-ion battery cathode materials. *Batteries* **2023**, *9*, 156. [[CrossRef](#)]
- Hasagawa, G.; Kuwata, N.; Tanaka, Y.; Miyazaki, T.; Ishigaki, N.; Takada, K.; Kawamura, J. Tracer diffusion coefficients of Li^+ ions in *c*-axis oriented Li_xCoO_2 thin films measured by secondary ion mass spectrometry. *Phys. Chem. Chem. Phys.* **2021**, *23*, 2438–2448. [[CrossRef](#)]
- Uxa, D.; Hüger, E.; Meyer, K.; Dörrer, L.; Schmidt, H. Lithium-ion diffusion in near-stoichiometric polycrystalline and monocrystalline LiCoO_2 . *Chem. Mater.* **2023**, *35*, 3307–3315. [[CrossRef](#)]
- Kawashima, K.; Ohnishi, T.; Takada, K. High-Rate Capability of LiCoO_2 Cathodes. *ACS Appl. Energy Mater.* **2020**, *3*, 11803–11810. [[CrossRef](#)]
- Uxa, D.; Holmes, H.J.; Meyer, K.; Dörrer, L.; Schmidt, H. Lithium Tracer Diffusion in Sub-Stoichiometric Lithium-Metal-Oxide Compounds. *Defect Diffus. Forum* **2021**, *413*, 125–135. [[CrossRef](#)]
- Bumberger, A.E.; Boehme, C.; Ring, J.; Raznjevic, S.; Zhang, Z.; Kubicek, M.; Fleig, J. Mass and Charge Transport in $\text{Li}_{1-\delta}\text{CoO}_2$ Thin Films—A Complete Set of Properties and Its Defect Chemical Interpretation. *Chem. Mater.* **2022**, *34*, 10548–10560. [[CrossRef](#)] [[PubMed](#)]
- Hüger, E.; Uxa, D.; Schmidt, H. Electrochemical (PITT, EIS) and Analytical (SIMS) Determination of Li Diffusivities at the Onset of Charging $\text{LiNi}_{0.33}\text{Mn}_{0.33}\text{Co}_{0.33}\text{O}_2$ Electrodes. *J. Phys. Chem. C* **2024**, *128*, 7408–7423. [[CrossRef](#)]
- Randles, J.E.B. Kinetics of rapid electrode reactions. *Discuss. Faraday Soc.* **1947**, *1*, 11–19. [[CrossRef](#)]
- Ho, C.; Raistrick, I.D.; Huggins, R.A. Application of A–C techniques to the study of lithium: Diffusion in tungsten trioxide thin films. *J. Electrochem. Soc.* **1980**, *127*, 343–350. [[CrossRef](#)]

12. Dawson, J.L.; John, D.G. Diffusion impedance—An extended general analysis. *J. Electroanal. Chem.* **1980**, *110*, 37–47. [CrossRef]
13. Macdonald, J.R. *Impedance Spectroscopy: Emphasizing Solid Materials and Systems*; John Wiley & Sons: Chichester, UK, 1987; ISBN 0-471-83122-0.
14. Taylor, S.R.; Gileadi, E. Physical interpretation of the Warburg impedance. *Corrosion* **1995**, *51*, 664–671. [CrossRef]
15. Muralidharan, V.S. Warburg impedance—Basics revisited. *Anti-Corros. Methods Mater.* **1997**, *44*, 26–29. [CrossRef]
16. Jamnik, J.; Maier, J.; Pejovnik, S. A powerful electrical network model for the impedance of mixed conductors. *Electrochim. Acta* **1999**, *44*, 4139–4145. [CrossRef]
17. Jamnik, J.; Maier, J. Generalised equivalent circuits for mass and charge transport: Chemical capacitance and its implications. *Phys. Chem. Chem. Phys.* **2001**, *3*, 1668–1678. [CrossRef]
18. Lai, W.; Haile, S.M. Impedance spectroscopy as a tool for chemical and electrochemical analysis of mixed conductors: A case study of ceria. *J. Am. Ceram. Soc.* **2005**, *88*, 2979–2997. [CrossRef]
19. Go, J.; Pyun, S. A review of anomalous diffusion phenomena at fractal interface for diffusion-controlled and non-diffusion-controlled transfer processes. *J. Solid State Electrochem.* **2007**, *11*, 323–334. [CrossRef]
20. Barbero, G.; Lelidis, I. Analysis of Warburg’s impedance and its equivalent electric circuits. *Phys. Chem. Chem. Phys.* **2017**, *19*, 24934. [CrossRef]
21. Nguyen, T.Q.; Breitkopf, C. Determination of diffusion coefficients using impedance spectroscopy data. *J. Electrochim. Soc.* **2018**, *165*, E826–E831. [CrossRef]
22. BioLogic. How to Interpret Lower Frequencies Impedance in Batteries? EC-Lab—Application Note 61. 2017. Available online: <https://www.biologic.net/documents/eis-low-frequencies-diffusion-battery-application-note-61/> (accessed on 20 February 2024).
23. BioLogic. Determination of the Diffusion Coefficient of an Inserted Species in a Host Electrode with EIS, PITT and GITT Techniques Battery—Application Note 70. 2024. Available online: <https://www.biologic.net/documents/determination-diffusion-coefficient-inserted-species-host-electrode-eis-pitt-gitt-techniques-an70/> (accessed on 29 October 2024).
24. Diard, J.P.; Le Gotrech, B.; Montella, C. *Handbook of Electrochemical Impedance Spectroscopy. Diffusion Impedances*; Technical Report; ER@SE/LEPMI: Grenoble, France, 2020; pp. 1–39. [CrossRef]
25. Meddings, N.; Heinrich, M.; Overney, F.; Lee, J.; Ruiz, V.; Napolitano, E.; Seitz, S.; Hinds, G.; Raccichini, R.; Gaberscek, M.; et al. Application of electrochemical impedance spectroscopy to commercial Li-ion cells: A review. *J. Power Sources* **2020**, *480*, 228742. [CrossRef]
26. Charbonneau, V.; Lasia, A.; Brisard, G. Impedance studies of Li⁺ diffusion in nickel manganese cobalt oxide (NMC) during charge/discharge cycles. *J. Electroanal. Chem.* **2020**, *875*, 113944. [CrossRef]
27. Janssen, M.; Bisquert, J. Locating the frequency of turnover in thin-film diffusion impedance. *J. Phys. Chem. C* **2021**, *125*, 15737–15741. [CrossRef]
28. Bumberger, A.E.; Boehme, C.; Ring, J.; Raznjevic, S.; Zhang, Z.; Kubicek, M.; Fleig, J. Defect chemistry of spinel cathode materials—A case study of epitaxial LiMn₂O₄ thin films. *Chem. Mater.* **2023**, *35*, 5135–5149. [CrossRef]
29. Lazanas, A.C.; Prodromidis, M.I. Electrochemical impedance spectroscopy: A tutorial. *ACS Meas. Sci. Au* **2023**, *3*, 162–193. [CrossRef] [PubMed]
30. Bisquert, J.; Garcia-Belmonte, G.; Bueno, P.; Longo, E.; Bulhoes, L.O.S. Impedance of constant phase element (CPE)-blocked diffusion in film electrodes. *J. Electroanal. Chem.* **1998**, *452*, 229–234. [CrossRef]
31. Bisquert, J.; Garcia-Belmonte, G.; Fabregat-Santiago, F.; Bueno, P.R. Theoretical models for ac impedance of finite diffusion layers exhibiting low frequency dispersion. *J. Electroanal. Chem.* **1999**, *475*, 152–163. [CrossRef]
32. Moya, A.A. Comparing the characteristic frequencies of the transmissive and reflexive finite-length Warburg diffusion processes. *J. Electroanal. Chem.* **2023**, *929*, 117132. [CrossRef]
33. Montella, C. Discussion of the potential step method for the determination of the diffusion coefficients of guest species in host materials Part I. Influence of charge transfer kinetics and ohmic potential drop. *J. Electroanal. Chem.* **2002**, *518*, 61–83. [CrossRef]
34. Weppner, W.; Huggins, R.A. Determination of the kinetic parameters of mixed-conducting electrodes and application to the system Li₃Sb. *J. Electrochem. Soc.* **1977**, *124*, 1569–1578. [CrossRef]
35. Uxa, D.; Hüger, E.; Schmidt, H. Li Diffusion in Thin Film LiySi Electrodes: Galvanostatic intermittent titration technique and tracer diffusion experiments. *J. Phys. Chem. C* **2020**, *124*, 27894–27899. [CrossRef]
36. McPhail, D.S. Applications of Secondary Ion Mass Spectrometry (SIMS) in Materials Science. *J. Mater. Sci.* **2006**, *41*, 873–903. [CrossRef]
37. Wilson, R.G. SIMS quantification in Si, GaAs, and diamond—An update. *Int. J. Mass Spectrom. Ion Process.* **1995**, *143*, 43–49. [CrossRef]
38. Stevie, F.A.; Griffis, D.P. Quantification in dynamic SIMS: Current status and future needs. *Appl. Surf. Sci.* **2008**, *255*, 1364–1367. [CrossRef]
39. Bianchini, M.; Roca-Ayats, M.; Hartmann, P.; Brezesinski, T.; Janek, J. There and back again—The journey of LiNiO₂ as a cathode active material. *Angew. Chem. Int. Ed.* **2019**, *58*, 10434–10458. [CrossRef] [PubMed]
40. Van der Ven, A.; Ceder, G. Lithium diffusion in layered Li_xCoO₂. *Electrochim. Solid-State Lett.* **2000**, *3*, 301. [CrossRef]
41. Uxa, D.; Holmes, H.; Meyer, K.; Dörrer, L.; Schmidt, H. Lithium tracer diffusion in LiNi_{0.33}Mn_{0.33}Co_{0.33}O₂ cathode material for lithium-ion batteries. *Phys. Chem. Chem. Phys.* **2021**, *23*, 5992. [CrossRef] [PubMed]

42. Wang, J.W.; He, Y.; Fan, F.; Liu, X.H.; Xia, S.; Liu, Y.; Harris, C.T.; Li, H.; Huang, J.Y.; Mao, S.X.; et al. Two-Phase Electrochemical Lithiation in Amorphous Silicon. *Nano Lett.* **2013**, *13*, 709–715. [[CrossRef](#)]
43. Uxa, D.; Jerliu, B.; Hüger, E.; Dörrer, L.; Horisberger, M.; Stahn, J.; Schmidt, H. On the lithiation mechanism of amorphous silicon electrodes in Li-ion batteries. *J. Phys. Chem. C* **2019**, *123*, 22027–22039. [[CrossRef](#)]
44. Lu, X.; Sun, Y.; Jian, Z.; He, X.; Gu, L.; Hu, Y.; Li, H.; Wang, Z.; Chen, W.; Duan, X.; et al. New Insight into the Atomic Structure of Electrochemically Delithiated $O_3\text{-Li}_{(1-x)}\text{CoO}_2$ ($0 \leq x \leq 0.5$) Nanoparticles. *Nano Lett.* **2012**, *12*, 6192–6197. [[CrossRef](#)]
45. Lin, C.; Li, J.; Yin, Z.; Huang, W.; Zhao, Q.; Weng, Q.; Liu, Q.; Sun, J.; Chen, G.; Pan, F. Structural Understanding for High-Voltage Stabilization of Lithium Cobalt Oxide. *Adv. Mater.* **2024**, *36*, 2307404. [[CrossRef](#)]

Disclaimer/Publisher’s Note: The statements, opinions and data contained in all publications are solely those of the individual author(s) and contributor(s) and not of MDPI and/or the editor(s). MDPI and/or the editor(s) disclaim responsibility for any injury to people or property resulting from any ideas, methods, instructions or products referred to in the content.